



1     **Increased surface water evaporation loss induced by**  
2         **reservoir development on the Loess Plateau**

3  
4

5     **Yao Liu<sup>1,2</sup>, Xianhong Xie<sup>1,2,\*</sup>, Yibing Wang<sup>1,2</sup>, Arken Tursun<sup>1,2</sup>, Dawei**  
6                     **Peng<sup>1,2</sup>, Xinran Wu<sup>1,2</sup>**

7     1. State Key Laboratory of Remote Sensing Science, Faculty of Geographical Science,  
8         Beijing Normal University, Beijing 100875, China  
9     2. Beijing Engineering Research Center for Global Land Remote Sensing Products,  
10         Faculty of Geographical Science, Beijing Normal University, Beijing 100875,  
11         China

12  
13  
14

15     \*Corresponding author:

16                     Xianhong Xie (Beijing Normal University, [xianhong@bnu.edu.cn](mailto:xianhong@bnu.edu.cn))  
17



## 1    Abstract

2        Global-scale reservoir construction has significantly enhanced local water supply  
3        for local production and livelihoods, yet the evaporation losses from these surface water  
4        bodies remain poorly understood, particularly in the context of climate change. The  
5        majority of existing studies have predominantly focused on terrestrial evaporation,  
6        overlooking the intricate evaporation dynamics within these aquatic systems. This  
7        study addresses this gap by investigating water body evaporation in the Loess Plateau  
8        of China, a region characterized by extensive reservoir development over the past  
9        decades. By employing a modified Penman equation and utilizing long-term remote  
10      sensing water body data to calculate water depths while accounting for the thermal  
11      storage capacity of water bodies, we estimated water evaporation rates and total  
12      evaporation volumes for the period 2000-2018. Validation against pan evaporation  
13      observations demonstrates the efficacy of our improved approach in capturing the  
14      evaporation patterns of diverse water bodies in the Loess Plateau. Results reveal a  
15      subtle decreasing trend in evaporation rates across the region. However, the total  
16      evaporation volume amounts to a substantial  $4.16 \times 10^6 \text{ m}^3/\text{d}$ , with a notable upward  
17      trend at a rate of  $0.117 \times 10^6 \text{ m}^3/\text{d/yr}$ . Attribution analysis shows that while the combined  
18      effects of climate change marginally reduced evaporation rates, the expansion of water  
19      bodies has counteracted this trend, resulting in a significant increase in total evaporation  
20      losses. Particularly, the development of small- and medium-sized reservoirs and check  
21      dams is the primary driver of increased evaporation losses on the Loess Plateau. Given  
22      comparable evaporation losses to surface water withdrawals in this region, future water



1 management and hydraulic projects must consider such substantial losses. This study  
2 fills gaps in evaporation dynamics and underscores the need for integrated strategies  
3 addressing climate change, reservoir expansion, and evaporation.

4 **Keywords:**

5 Surface water area; Water depth; Evaporation estimation; Evaporation volume;  
6 Reservoir development; Remote sensing;

7



## 1 1. Introduction

2 Land surface water bodies, such as reservoirs and lakes, serve as vital sources of  
3 'blue water' that sustain human livelihoods and production, while their evaporation  
4 processes exert significant influence on climate regulation and land surface energy  
5 partitioning across the land surface (Guan and Mascaro, 2023). A large number of  
6 studies have been predominantly focused on evaporation from vegetation and soil  
7 profile (Jian et al., 2015; Liu et al., 2024; Peng et al., 2024), with scant attention given  
8 to the evaporation loss from surface water bodies. Globally, reservoir storage increased  
9 rapidly at a rate of  $27.82 \text{ km}^3$  per year from 1999 to 2018, driven by the construction of  
10 thousands of new reservoirs to address rising demands for water supply, irrigation, and  
11 energy (Li et al., 2023). However, it has been reported that large reservoirs globally  
12 evaporated about  $340 \text{ km}^3/\text{yr}$  from 1985 to 2016, which is over 70% of the amount of  
13 municipal water withdrawal in 2010 (Tian et al., 2022). Moreover, the long-term  
14 average evaporation volume from lakes worldwide is estimated to be approximately  
15  $1500 \pm 150 \text{ km}^3/\text{yr}$  (Zhao et al., 2022). Therefore, the impact of water body evaporation  
16 losses on human society should not be underestimated.

17 Surface/open water evaporation is influenced by a range of meteorological factors  
18 and water surface conditions. These include near-surface air temperature, relative  
19 humidity, solar shortwave radiation, and the temperature profile within water bodies  
20 (Milly and Dunne, 2020; Vystavna et al., 2021). Variations in these factors elicit  
21 corresponding changes in both the evaporation rate and evaporation volume. For



1 instance, an elevation in near-surface air temperature over the lakes of the Yunnan-  
2 Guizhou Plateau has led to accelerated evaporation rates (Yang et al., 2019). Beyond  
3 these meteorological factors, changes in surface water area also play a crucial role in  
4 determining evaporation losses. As an illustration, the total evaporation volume from  
5 reservoirs in China has risen, with 96% of this increase attributed to newly constructed  
6 reservoirs (Tian et al., 2021). Similarly, in the United States, while rising temperatures  
7 have contributed to an increase in total evaporation loss from reservoirs, this effect has  
8 been largely counteracted by a decrease in surface area (Zhao and Gao, 2019). Another  
9 example is the evaporation rates at Siling Co Lake on the Tibetan Plateau, which have  
10 decreased partially due to lower wind speeds, contributing to the expansion of the lake  
11 surface area (Guo et al., 2019).

12 In recent decades, the Loess Plateau in China has experienced significant climatic  
13 shifts, accompanied by substantial variations in vegetation cover (Jiang et al., 2021; Wu  
14 et al., 2020; Xie et al., 2015). A notable observation is the enhancement of land surface  
15 evaporation, particularly attributed to increased vegetation transpiration (Jiang et al.,  
16 2022; Peng et al., 2024). Key climate factors such as temperature, radiation, and wind  
17 speed all play crucial roles in this process (Bai et al., 2019; Jin et al., 2017; Li et al.,  
18 2009). However, it is imperative to recognize that water body evaporation is also a vital  
19 component of the water cycle on the Loess Plateau, necessitating a closer examination  
20 of its dynamics. Moreover, to mitigate soil erosion and reduce the sediment content, a  
21 variety of large, medium and small-scale dam and reservoir projects have been  
22 carried out on a large scale (Fu et al., 2017). These interventions have led to notable



1 changes in the water landscape (Liu et al., 2023). This substantial expansion of surface  
2 water bodies is expected to enhance water retention, thereby supporting human  
3 livelihoods and production (Woolway et al., 2020; Zhou et al., 2020). However, it may  
4 also exacerbate water evaporation losses, particularly under the arid climatic conditions  
5 of the Loess Plateau, which can further accelerate surface water evaporation.  
6 Consequently, amidst ongoing climate change and alterations in water body area, there  
7 is a pressing need to deepen our understanding of the evolving patterns of water body  
8 evaporation, both in terms of rate and volume.

9 Several methods are accessible for estimating surface water evaporation, including  
10 the pan measurement, eddy covariance observation (EC), and hydrological model  
11 simulations (Friedrich et al., 2018; Hollinger and Richardson, 2005; Liu et al., 2012;  
12 Rotstayn et al., 2006; Woolway et al., 2020). Among these approaches, the hydrological  
13 modeling stands out due to its ability to integrate various meteorological and  
14 hydrological factors (Deng et al., 2022; Vishwakarma et al., 2022). This approach  
15 simulates evaporation processes across diverse environmental conditions, rendering it  
16 suitable for large-scale regions and long-term predictions. Notably, the Penman  
17 equation is widely preferred owing to its straightforward application principles, high  
18 degree accuracy, and broad applicability (Fuentes et al., 2020; McJannet et al., 2008;  
19 Tanny et al., 2008). However, a significant challenge arises from the fact that water  
20 possesses a significantly higher heat capacity compared to other land types, resulting in  
21 pronounced heat storage effects in lakes and reservoirs (Jensen, 2010). The thermal  
22 energy within these water bodies tends to move from shallower to deeper regions (Wang



1 et al., 2023), consequently influencing evaporation, sensible heat flux, and net  
2 longwave radiation losses at the surface. To address biases in evaporation rate  
3 estimations stemming from these factors, Edinger et al. (1968) introduced the concept  
4 of equilibrium temperature. Subsequently, De Bruin (1982) incorporated this concept  
5 into the estimation of evaporation rates. Zhao and Gao (2019) further enhanced  
6 evaporation estimations in open water by establishing a generalized formula for  
7 equilibrium temperature, where water depth emerged as a crucial parameter for  
8 estimating equilibrium temperature.

9 With advancement of remote sensing technology and modern measurement  
10 techniques, lakes and reservoirs have been comprehensive measurement and scrutiny,  
11 spanning from local basins to national and even global scales (Li et al., 2020; Zhang et  
12 al., 2019a). Despite these advancements, existing research primarily utilizes remote  
13 sensing data to calculate changes in surface water area, while there is a notable absence  
14 of accessible data for estimating surface water evaporation losses, such as water depth  
15 information. Consequently, while the Penman equation offers numerous advantages, its  
16 application in hydrological models does have limitations, particularly in accurately  
17 accounting for the complex thermal dynamics of water bodies.

18 The objective of this study is to integrate remote sensing data with an open water  
19 evaporation model to assess evaporation losses on the Loess Plateau. Utilizing a  
20 modified Penman equation, which estimates surface water evaporation based on  
21 equilibrium temperature, and incorporating a water depth calculation, this study  
22 comprehensively accounts for variations in water body characteristics, notably water



1 depth and surface area. This enhanced methodology aims to achieve a more reliable  
2 estimation of energy fluctuations arising from water body heat storage, thereby  
3 providing a thorough assessment of regional-scale water evaporation losses. This  
4 assessment is crucial for facilitating effective regional or local water resource  
5 management. The primary research objectives are twofold: 1) to estimate the spatial  
6 and temporal variability of surface water evaporation rates and volumes on the Loess  
7 Plateau, and 2) to identify the key driving factors underlying surface water evaporation  
8 losses, with a particular emphasis on the influence of surface water bodies.

## 9 **2. Data and Methods**

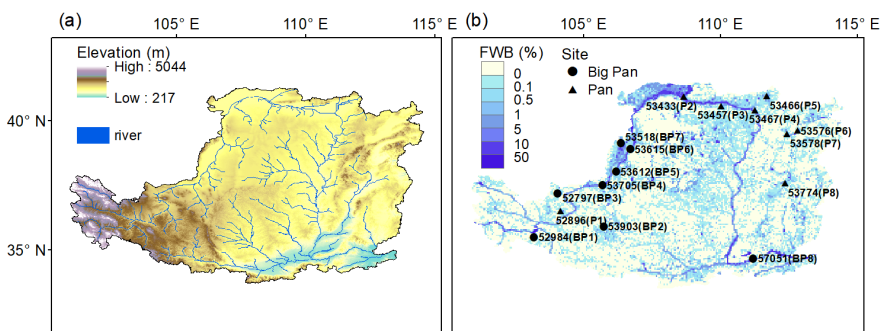
### 10 **2.1 Study area**

11 The Loess Plateau is located in the northwestern region of China, with an area of  
12 approximately 640,000 km<sup>2</sup>. Influenced by summer monsoon from the southeast, its  
13 climatic conditions in the area show a gradual change from southeast to northwest.  
14 Annual precipitation shows a decreasing trend following this spatial pattern with an  
15 area-average precipitation of about 440 mm. Meanwhile, seasonal characteristics are  
16 significant, with rain and heat coinciding, rainfall is mainly concentrated in summer in  
17 the form of heavy rainfall (60–70%) (Jiang et al., 2021; Sun et al., 2015). The region is  
18 predominantly located within the Yellow River basin (Fig. 1a), encompassing  
19 subsidiary rivers such as the Wei River. However, the overall availability of surface  
20 water resources is still relatively scarce (Xiao et al., 2019).

21 Characterized by its loose soil structure, the Loess Plateau makes it highly



1 susceptible to severe soil erosion due to wind and water (Jiang et al., 2019; Zhao et al.,  
2 2013). In order to retain soil and sediment and to reduce the amount of sediment load  
3 to the main channel, a large amount of small-scale check dams have been constructed  
4 within gullies and small tributaries on the Loess Plateau after 2000 (Wang et al., 2021;  
5 Zhang et al., 2022). Driven by the economic development of agriculture, industry, and  
6 various sectors, there has been a heightened demand for water resources. Consequently,  
7 hydraulic infrastructure including reservoirs, has been continuously expanding.  
8 permanent water bodies on the Loess Plateau grow from 1,200 km<sup>2</sup> in 2000 to 2,200  
9 km<sup>2</sup> in 2020, and the number of small water bodies has increased from 6,721 to 14,082  
10 (Liu et al., 2023). Furthermore, there is a widespread distribution of agricultural  
11 irrigation districts in the western and northern regions of the Loess Plateau, etc.,  
12 Ningxia Irrigation District and Hetao Irrigation District (Zhang et al., 2019). All of these  
13 factors collectively influence the fraction of surface water bodies in the Loess Plateau  
14 (Fig. 1b).



15  
16 **Fig. 1.** Location of the Loess Plateau and its water body distribution: (a) Elevation and  
17 river systems of the Loess Plateau; and (b) Distribution of evaporation measurement  
18 sites for big pan and pan, and fraction of water body (FWB) on the Loess Plateau.



## 1    2.2 Data

2       The data used in this study include remote sensing surface water area,  
3       meteorological forcing, and other ancillary information. Monthly surface water area  
4       data for the Loess Plateau were obtained from the Joint Research Center (JRC) Global  
5       Surface Water dataset (GSW) (Pekel et al., 2016). This dataset utilized an expert system  
6       classifier based on Landsat satellite imagery to map the spatial dynamics of global  
7       surface water, with a spatial resolution of 30 m. The JRC-GSW data have been  
8       successfully applied to detect changes in surface water in the Loess Plateau (Liu et al.,  
9       2023). The driving meteorological data used for surface water evaporation estimation  
10      include temperature, specific humidity, shortwave radiation, and wind speed, sourced  
11      from the China Meteorological Forcing Dataset (CMFD) (He et al., 2020) with a spatial  
12      resolution of 0.1°. The CMFD data have undergone comprehensive validation in China  
13      with reliable performance (Lei et al., 2023; Tan et al., 2021; Wang et al., 2024; Zhang  
14      et al., 2023). Additionally, surface wind speed data from ECMWF Reanalysis 5th  
15      Generation (ERA5) (Hersbach et al., 2020) were employed to determine the prevailing  
16      wind direction, which was then used to calculate downwind width of water bodies. The  
17      ancillary data regarding elevation information were from Advanced Spaceborne  
18      Thermal Emission and Reflection Radiometer Global Digital Elevation Model  
19      (ASTGTM), available at <https://lpdaac.usgs.gov/products/astgtmv003/>. This dataset has  
20      a horizontal spatial resolution of 30 m and a vertical resolution of 1 m.

21       We obtained open-water evaporation observations from China Meteorological  
22      Administration (<http://data.cma.cn/>). The observation of the evaporation was



1 performed using big pan (E601) and small pan with diameter of 20 cm. Given the  
2 difference between the evaporation from the pan and the near water body, a few studies  
3 adjusted the observations using pan coefficients so that the observations is comparable  
4 with the evaporation from the near water body (Jinhui and Zhanbin, 2007; Li et al.,  
5 2018; Sheng et al., 2007). Pan coefficients may vary with the size of the pan and the  
6 seasons. Shi et al. (1986) proposed specific pan coefficients that are suitable for  
7 different regions in China. Based on the study, we set the pan coefficient as 0.95 for the  
8 E601 and 0.75 for the small pan observations, which have been successfully used in  
9 reservoir evaporation estimation in the upper Yellow River (Bai et al., 2023).

10 **2.3 Evaporation estimation**

11 **2.3.1 Evaporation rate**

12 To account for the effect of heat storage in a water body, we proposed a modified  
13 Penman equation that incorporates water depth into the heat storage estimation, thereby  
14 enabling more accurate computation of surface water evaporation (Penman, 1948). This  
15 equation follows the traditional Penman equation, and explicitly considers the heat  
16 storage:

$$17 E = \frac{s(R_n - \Delta U) + \gamma f(u)(e_s - e_a)}{\lambda_v(s + \gamma)} \quad (1)$$

18 where  $E$  is the evaporation rate ( $\text{mm} \cdot \text{d}^{-1}$ ),  $s$  is the slope of the saturation vapor  
19 pressure curve ( $\text{kPa} \cdot \text{C}^{-1}$ );  $R_n$  is the net radiation ( $\text{MJ} \cdot \text{m}^{-2} \cdot \text{d}^{-1}$ );  $\Delta U$  is the heat  
20 storage changes of the water body ( $\text{MJ} \cdot \text{m}^{-2} \cdot \text{d}^{-1}$ );  $f(u)$  is the wind function ( $\text{MJ} \cdot$   
21  $\text{m}^{-2} \cdot \text{d}^{-1} \cdot \text{kPa}^{-1}$ );  $e_s$  is the saturated vapor pressure at air temperature (kPa);  $e_a$  is  
22 the air vapor pressure (kPa);  $\lambda_v$  is the latent heat of vaporization ( $\text{MJ} \cdot \text{kg}^{-1}$ ); and  $\gamma$



1 is the psychrometric constant ( $\text{kPa} \cdot ^\circ\text{C}^{-1}$ ).

2 In the Penman equation, it is assumed that the input meteorological variables are  
3 derived from the surface water. However, due to data limitations, we can only obtain  
4 meteorological data based on land surface observations. To address the errors associated  
5 with the land-based meteorological data, Mcjannet et al., (2012) developed a widely  
6 used wind function:

7 
$$f(u_2) = \lambda_v(2.33 + 1.65u_2)L_f^{-0.1} \quad (2)$$

8 where  $f(u_2)$  is the wind function ( $\text{MJ} \cdot \text{m}^{-2} \cdot \text{d}^{-1} \cdot \text{kPa}^{-1}$ );  $u_2$  is the wind speed at  
9 the height of 2 m ( $\text{m} \cdot \text{s}^{-1}$ );  $L_f$  is the fetch length of the water body (m), fetch length  
10 is the surface water width under prevailing wind direction.

11 Another key factor affecting estimation accuracy arises from variations in the  
12 energy stored within the water body. The introduction of equilibrium temperature serves  
13 as an effective solution (De Bruin, 1982; McMahon et al., 2013). Here, we utilize the  
14 more general equilibrium temperature formula derived by Zhao and Gao (2019):

15 
$$T_e = \frac{[k\varepsilon_a + f(u) \cdot (s + \gamma)] \cdot T_a + (1 - \alpha)K \downarrow - b(\varepsilon_w - \varepsilon_a) - f(u)(e_s - e_a)}{k\varepsilon_w + f(u) \cdot (s + \gamma)} \quad (3)$$

16 where  $T_e$  is the equilibrium temperature ( $^\circ\text{C}$ );  $\varepsilon_a$  and  $\varepsilon_w$  are emissivity of air and  
17 water with cloudiness factor, respectively;  $k$  and  $b$  are constants of  $0.46 \text{ MJ} \cdot \text{m}^{-2} \cdot$   
18  $\text{d}^{-1} \cdot ^\circ\text{C}^{-1}$  and  $23.38 \text{ MJ} \cdot \text{m}^{-2}$ , respectively. Based on such equilibrium temperature,  
19 the water temperature can be estimated as

20 
$$T_w = T_e + (T_{w0} - T_e) \cdot e^{-\frac{\Delta t}{\tau}} \quad (4)$$

21 where  $T_w$  is the water column temperature at the current time step ( $^\circ\text{C}$ );  $T_{w0}$  is the  
22 water column temperature at the previous time step ( $^\circ\text{C}$ );  $\Delta t$  is the time step (set as



1 one month in this study); and  $\tau$  is the lag time (d), can be expressed as

2

$$\tau = \frac{\rho_w c_w \bar{h}}{4\sigma(T_{wb} + 273.15)^3 + f(u)(s_{wb} + \gamma)} \quad (5)$$

3 where  $\rho_w$  is the water density ( $\text{kg} \cdot \text{m}^{-3}$ );  $c_w$  is the specific heat of water ( $\text{MJ} \cdot \text{kg}^{-1} \cdot$   
4  $^{\circ}\text{C}^{-1}$ );  $\bar{h}$  is the average water depth (m);  $T_{wb}$  is the wet-bulb temperature ( $^{\circ}\text{C}$ ); and  
5  $s_{wb}$  is the slope of the saturation vapor pressure curve at  $T_{wb}$  ( $\text{kPa} \cdot ^{\circ}\text{C}$ ).

6 The change in the heat storage of water is calculated by the difference in heat  
7 between the moments at the current time and initial time step, using the following  
8 equation:

9

$$\Delta U = \rho_w c_w \bar{h} \frac{T_w - T_{wo}}{\Delta t} \quad (6)$$

10 where  $\Delta U$  is the changes of water storage heat.

### 11 2.3.2 Water depth estimation

12 In the estimation of evaporation, accounting for water depth variation is crucial,  
13 as it fundamentally influences heat storage and transfer dynamics, as shown in  
14 Equations (5) and (6). A significant challenge arises in quantifying evaporation rates  
15 for surface water, largely attributed to the limited availability of comprehensive water  
16 depth data. Digital Elevation Models (DEMs), while valuable, are typically restricted  
17 to capturing surface-level information, thereby hindering the acquisition of detailed  
18 underwater terrain features. To circumvent this limitation, we proposed a water depth  
19 estimation algorithm that operates on the assumption of slope equivalence between the  
20 water body and its boundaries, as depicted in Figure 2. This approach first relies on the  
21 elevation and slope of the land pixels to estimate the water bottom elevation of the  
22 boundary water grids. All land pixels and the calculated water grids are marked as



1 known. Subsequently, the water bottom elevation of interior grids is iteratively  
2 determined using the same approach based on known neighboring grids within their  
3 eight-neighborhood.

4 For each grid cell (with a resolution of 30 m × 30 m), the determination of water  
5 bottom or bed elevation is expressed as:

$$6 H_w = \frac{\sum_{i=1}^n (H_i - \tan S_i \times D_i)}{n} \quad (7)$$

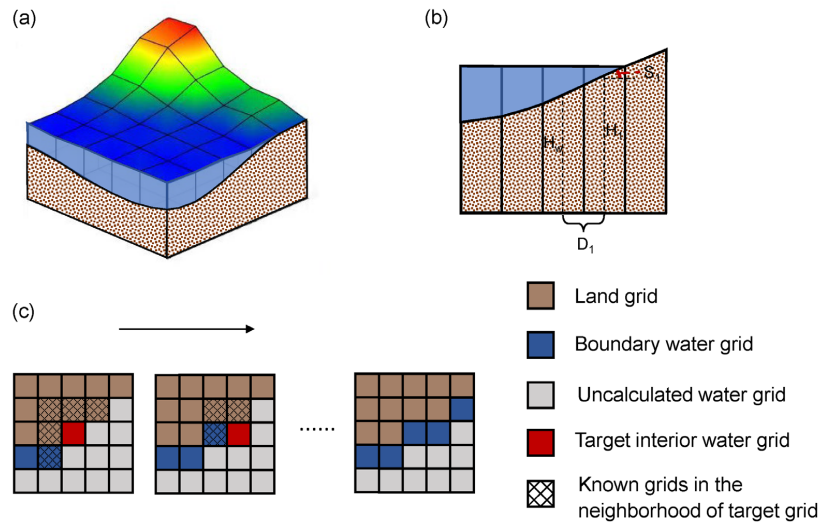
7 where,  $H_w$  is the water bottom elevation of a target grid cell with resolution of 30 m;  
8  $n$  is the total number of marked as known in the eight-neighborhood;  $H_i$  is the  $i^{th}$   
9 elevation value of the water body boundary or the already calculated elevation value of  
10 the water grid;  $S_i$  is the slope of the  $i^{th}$  grid;  $D_i$  is the distance from the  $i^{th}$  grid to the  
11 target water grid. The calculation for water body grid follows the rule of starting from  
12 the nearest grids to the water body boundary and progressing to the farthest ones.

13 For a given water body, its average water depth is defined as the difference  
14 between the mean elevation of the land boundary grids and the mean waterbed elevation  
15 of the water grids:

$$16 \bar{h} = \overline{H_b} - \overline{H_w} \quad (8)$$

17 where  $\bar{h}$  is the average water body depth;  $\overline{H_b}$  is the average elevation of the water  
18 body boundary;  $\overline{H_w}$  is the average elevation of the waterbed.

19



1

2 **Fig. 2.** The water bottom elevation calculation: (a) three-dimensional schematic of a  
3 water body, (b) longitudinal section view a water body, and (c) the iterative process of  
4 calculating the bottom elevation of water grids, which involves progressively  
5 computing based on the known elevations of the eight-neighboring grid points and  
6 extending step-by-step into the interior water grids.

7 **2.3.3 Evaporation volume**

8 The total evaporation volume (EV) or evaporation loss can be expressed as,

9 
$$EV = E \times Area \times 1000 \quad (9)$$

10 where  $EV$  is monthly average evaporation volume ( $m^3/d$ ),  $E$  is monthly average  
11 evaporation rate ( $mm/d$ ), and  $Area$  is surface water bodies area within each grid cell  
12 ( $km^2$ ).

13 **2.4 Attribution analysis**

1 The change in evaporation volume of a water body is generally driven by its  
2 surface water area and four climate factors, including air temperature, humidity, wind  
3 speed, and downward shortwave radiation. To quantify the impacts of these factors, we  
4 designed five simulation experiments corresponding to the five factors. In each of the  
5 experiments associated with climate change effect, we detrended one of the four factors  
6 by removing the linear variation of the annual averages, and kept the dynamics of the  
7 other three factors. The detrended equation is presented as

$$M_{Y_{i,d}}' = \left[ \frac{M_{Y_i} + \alpha \times (Y_p - Y_i)}{M_{Y_i}} \right] \times M_{Y_{i,d}} \quad (10)$$

9 where  $Y_i$  is one year from 2000 to 2018;  $M'_{Y_{i,d}}$  is the daily-scale meteorological  
 10 forcing variable (including temperature, wind speed, specific humidity, and shortwave  
 11 radiation) for  $Y_i$  after detrend;  $M_{Y_{i,d}}$  is the original daily-scale meteorological data;  
 12  $M_{Y_i}$  is the annual average meteorological data for the year  $Y_i$ ;  $Y_b$  is the reference year  
 13 in 2000, and  $\alpha$  is the trend in the annual average meteorological data. For the  
 14 experiment associated with the surface water area, the same equation can be used for  
 15 detrending the surface water area. However, since the surface water area is based on  
 16 monthly-scale data,  $M'_{Y_{i,d}}$ , and  $M_{Y_{i,d}}$  respectively denote the detrended monthly-scale  
 17 water area and the original water area, and the parameter of  $\alpha$  represents the trend  
 18 derived from the monthly-scale original water area. This equation is able to remove the  
 19 annual trend but preserve the seasonal variation. Based on the five experimental  
 20 simulations and the base simulation that estimate the long-term evaporation volume in  
 21 the study period, we can calculate the contribution of each factor as,

$$Con_x = \frac{Trend_{Ex} - Trend_{Ebase}}{Trend_{Eoriginal}} \times 100\% \quad (11)$$

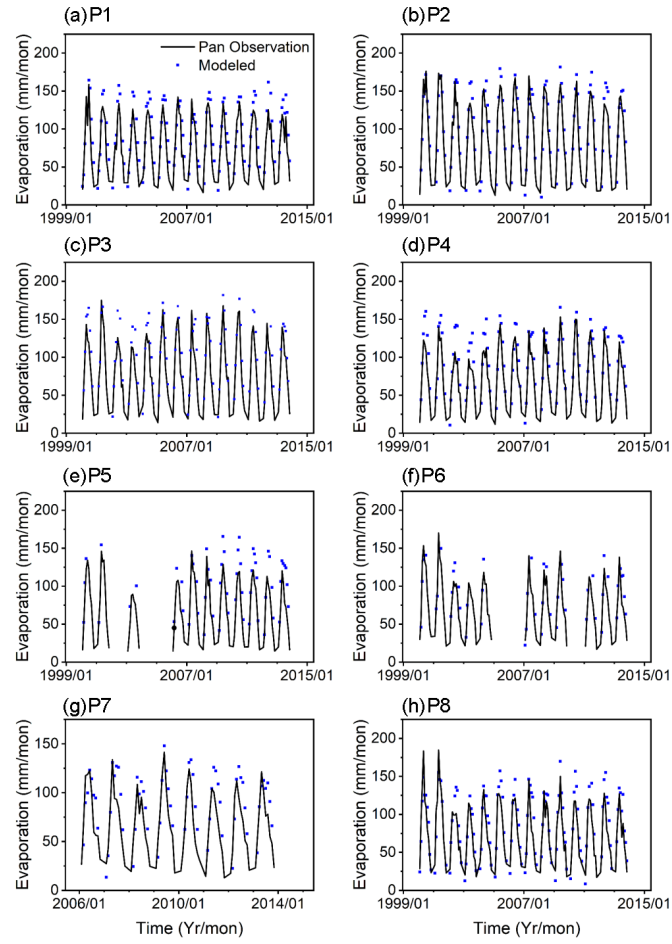


1 where  $Con_x$  is contribution percentage of the variation in element  $x$  (e.g.,  
2 temperature, specific humidity, shortwave radiation, wind speed, and surface water area)  
3 to the changes in  $EV$ ;  $Trend_{Ex}$  is the trend of  $EV$  after detrending all factors except  
4 for the element  $x$ ;  $Trend_{Ebase}$  is the trend of  $EV$  after detrending all factors; and  
5  $Trend_{Eoriginal}$  is the original trend of  $EV$ .

### 6 3. Results

#### 7 3.1 Evaluation of evaporation rate estimation

8 We first evaluate the evaporation estimation using the observations that have been  
9 adjusted as described in subsection 2.2. Figure 3 illustrates a comparison between the  
10 estimated evaporation from water bodies and the observations from the small-pan  
11 evaporation. The evaporation estimates exhibit a strong agreement with the  
12 observations, capturing the monthly dynamic changes. The overall coefficient of  
13 determination ( $R^2$ ) for this comparison is 0.75, indicating a robust correlation. The bias  
14 is minimal, with a value less than 5 mm/month, and the root mean square error (RMSE)  
15 stands at approximately 22.54 mm/month. However, at certain stations, such as station  
16 P6, the modified Penman equation slightly underestimates peak evaporation values.  
17 Nevertheless, the overall alignment is deemed acceptable.



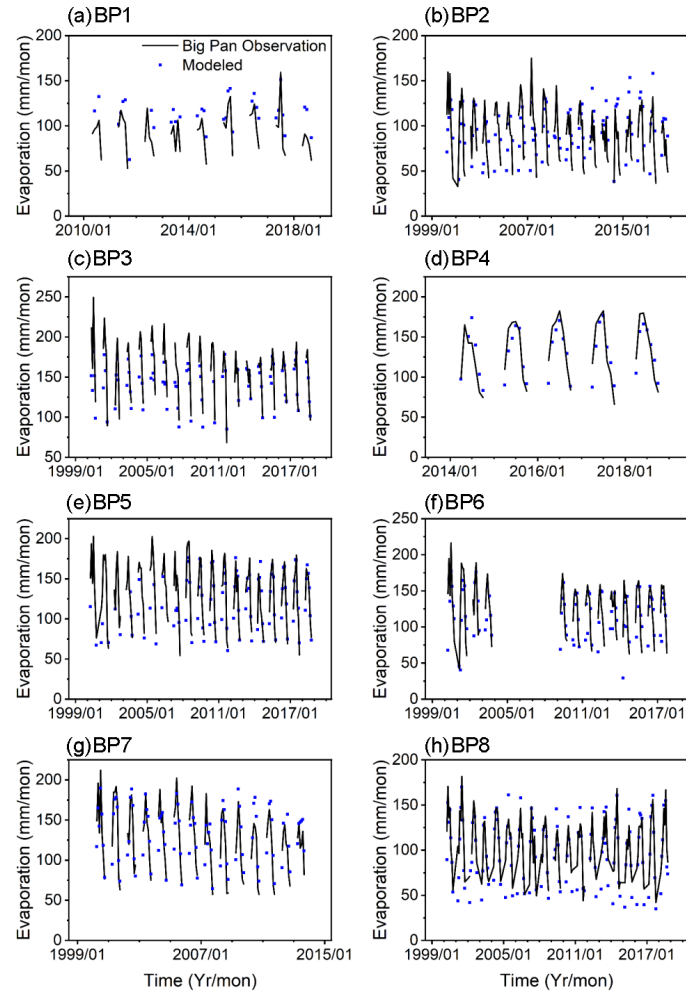
1

2 **Fig. 3.** Comparison of the estimated evaporation and the observations from small pan  
3 at eight stations: the plots from (a) to (h) are for the eight stations as shown in Figure 1.

4 Figure 4 provides a comparison between the estimated evaporation and the  
5 observations recorded by big pans. This comparison underscores a notable alignment,  
6 reflecting a coefficient of determination ( $R^2$ ) of 0.66. This strong correlation indicates  
7 that the model effectively captures the temporal variations in water body evaporation.  
8 Importantly, the performance metrics for the big-pan evaporation show an improvement



1 over those from the small pans. Specifically, the bias in the estimation for the big pans  
2 is lower, remaining well within 1 mm/month, and the root mean square error (RMSE)  
3 decreases to 22.50 mm/month, compared to the RMSE for the small pans in Figure 3.  
4 This enhanced accuracy can be attributed to several factors. Big evaporation pans, by  
5 their design, cover a greater surface area and thus provide a more representative  
6 measure of evaporation from larger water bodies. Their size likely mitigates the  
7 influence of localized environmental variabilities, such as temperature fluctuations and  
8 wind patterns, which can disproportionately affect smaller pans. Furthermore, the closer  
9 resemblance of big evaporation pans to actual water bodies in terms of surface area and  
10 heat exchange dynamics may contribute to their higher observational accuracy. This  
11 similarity likely reduces systematic errors and improves the overall agreement between  
12 simulated and observed evaporation rates.



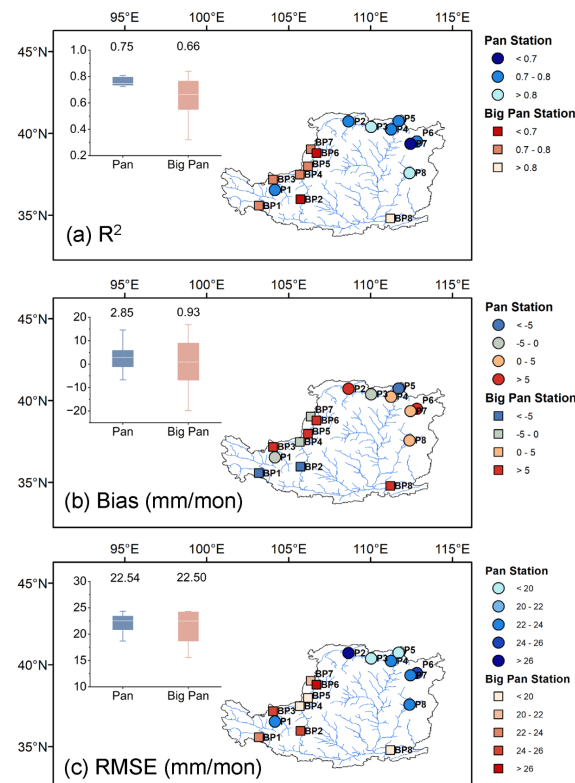
1

2 **Fig. 4.** Comparison of the estimated evaporation and the observations from big pan at  
3 eight stations: the plots from (a) to (h) are for the eight stations as shown in Figure 1.

4 Figure 5 presents the spatial distribution of  $R^2$ , Bias, and RMSE, offering a  
5 nuanced understanding of the model's performance across different regions. Notably,  
6 the upstream areas exhibit larger estimation errors, with bias exceeding 5 mm/month at  
7 three stations. This could be attributed to the complex terrain and lower temperatures



1 in these regions, which might introduce significant uncertainties in water depth  
2 calculations, subsequently affecting the accuracy of evaporation estimates. In contrast,  
3 the midstream and downstream regions demonstrate better accuracy, likely due to more  
4 homogeneous environmental conditions and milder temperature variations. The overall  
5 consistency between the simulated evaporation and the observations underscores the  
6 reliability of the modified Penman method for estimating evaporation, despite some  
7 localized discrepancies. This confirms the method's applicability for analyzing  
8 spatiotemporal variations in water body evaporation across the diverse landscapes of  
9 the Loess Plateau region.





1     **Fig. 5.** The spatial distribution and box plots of the three metrics (a) coefficient of  
2     determination ( $R^2$ ), (b) bias, and (c) root-mean-square error (RMSE) for simulated data  
3     comparing to pan and big pan.

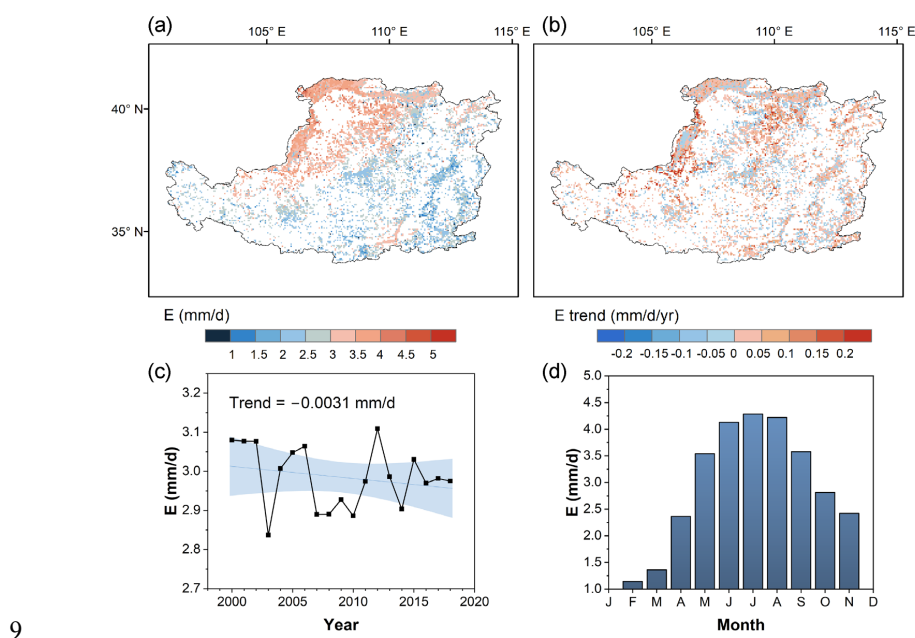
4     **3.2 Spatial-temporal variation in evaporation rate**

5           Evaporation from water bodies across the Loess Plateau demonstrates pronounced  
6     geographical heterogeneity. The spatial distribution of evaporation exhibits a gradual  
7     decrease from the northwest to the southeast, as depicted in Figure 6a. The long-term  
8     average evaporation rates vary between 2.8 and 3.1 mm/d, with certain areas in the  
9     northwest exceeding 5 mm/d. This spatial pattern suggests that regional climate  
10    conditions, including temperature, humidity, and wind speed, significantly influence  
11    evaporation rates. Temporal changes in evaporation, however, do not follow a  
12    discernible trend and appear relatively decentralized, as illustrated in Figure 6b. Despite  
13    this, areas experiencing decreasing evaporation are slightly more extensive than those  
14    with increasing evaporation. Notably, regions with significant increases in evaporation  
15    rates ( $p < 0.01$ ) are concentrated in the western and north-central parts of the Loess  
16    Plateau, indicating localized factors may be driving these increases, such as changes in  
17    water body characteristics.

18           Figure 6c and d present the interannual change and seasonality of evaporation rates.  
19    Over the period from 2000 to 2018, the long-term average daily evaporation rate on the  
20    Loess Plateau was approximately 2.98 mm/d. However, this rate decreased slightly at  
21    a rate of  $-0.0031$  mm/d/yr, indicating a subtle but consistent decline in evaporation over



1 the study period. The interannual variability in evaporation is substantial, with notable  
2 lows in 2003, when daily evaporation rates dropped to approximately 2.8 mm/d. This  
3 year likely experienced unusual climatic conditions that suppressed evaporation, such  
4 as increased cloud cover, reduced temperatures, or higher than average precipitation. In  
5 contrast, other years maintained average evaporation rates around 2.98 mm/d, reflecting  
6 the typical evaporative conditions of the region. Please note December and January  
7 were not considered for evaporation estimation in this study due to low temperatures  
8 and freezing of the water bodies.



9  
10 **Fig. 6.** The spatial distribution of (a) long-term average daily evaporation rate and (b)  
11 temporal trends. Average variations in evaporation rates for (c) annually dynamics and  
12 (d) monthly climatology.



### 1    3.3 Spatial-temporal variation in evaporation volume

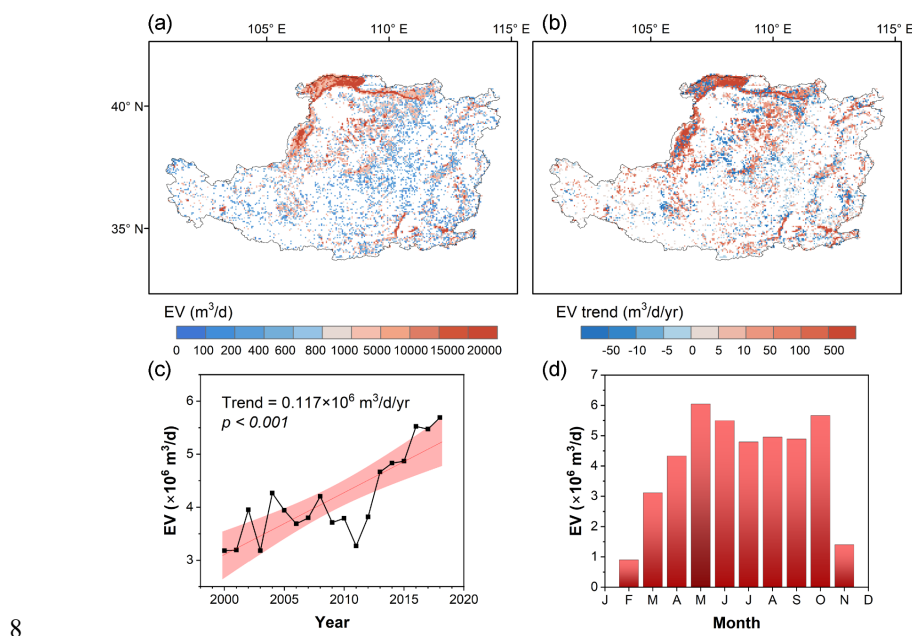
2       The spatial distribution of evaporation volume across the Loess Plateau is depicted  
3       in Fig. 7a, revealing a distinct pattern of high evaporation in the northwest and lower  
4       values in other regions. In the densely watered northwestern areas, evaporation volumes  
5       exceed 20,000 m<sup>3</sup>/d, contrasting sharply with most regions where evaporation remains  
6       below 1,000 m<sup>3</sup>/d. A notable increasing trend in evaporation volume is observed,  
7       particularly concentrated in the northwest (Fig. 7b), coinciding with areas experiencing  
8       high evaporation loss. Additionally, significant changes in surface water evaporation  
9       loss are evident in the southeastern and central-northern parts of the plateau, where the  
10      evaporation volume increased with the rate up to 100 m<sup>3</sup>/d/yr.

11      Figure 7c illustrates the temporal change in daily evaporation volume on the Loess  
12      Plateau. A significant upward trend ( $P < 0.01$ ) is observed, with an average annual  
13      increase of  $0.117 \times 10^6$  m<sup>3</sup>/d/yr. Evaporation volumes rose from  $3.18 \times 10^6$  m<sup>3</sup>/d in 2000  
14      to  $5.69 \times 10^6$  m<sup>3</sup>/d in 2018, with a long-term average of  $4.16 \times 10^6$  m<sup>3</sup>/d for the period  
15      2000-2018. Seasonal variation in evaporation volume exhibits distinct peaks in spring  
16      and autumn, with a yearly maximum of  $6.04 \times 10^6$  m<sup>3</sup>/d in May. It is noteworthy that  
17      while evaporation rates peak during the summer, evaporation volumes peak in May,  
18      aligning with seasonal fluctuations in water body areas (Liu et al., 2023). This implies  
19      that the seasonal variation in evaporation volume may be dominated by changes in  
20      surface water area.

21      An analysis of temporal fluctuations reveals inconsistencies between evaporation



1 loss and evaporation rate. Specifically, years with low evaporation loss, such as 2000,  
2 2001, 2003, and 2011, do not always correspond to years with low evaporation rates,  
3 which were 2003 and 2010. This discrepancy also suggests that factors other than  
4 meteorological conditions may control evaporation loss. The difference in patterns  
5 suggests that while evaporation rates are largely driven by climatic factors like  
6 temperature, humidity, and wind speed, evaporation loss may be more sensitive to  
7 changes in water body characteristics, such as surface area, depth, and water availability.



9 **Fig. 7.** The spatial distribution of (a) average evaporation volumes and (b) their  
10 temporal trends. Average variations in evaporation volumes for (c) annually and (d)  
11 monthly climatology.

### 12 3.4 Effect of driving factors on evaporation loss



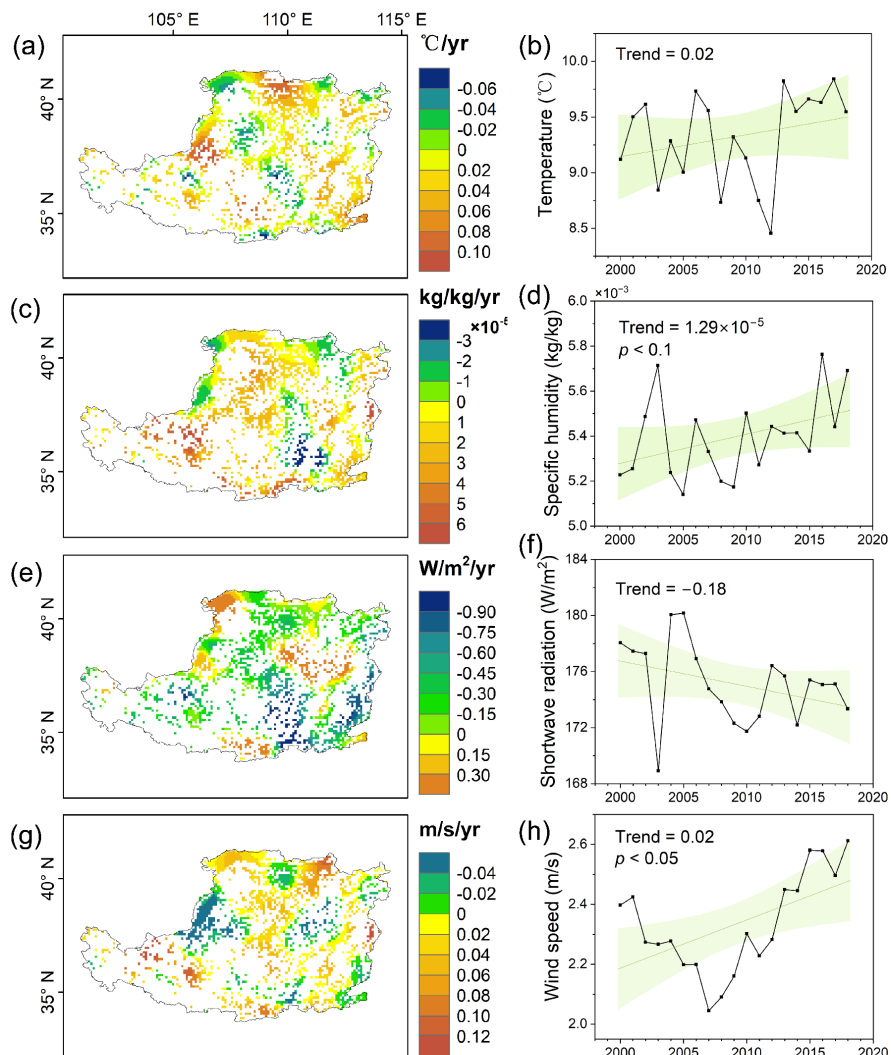
### 1    3.4.1    Dynamics of driving factors

2        Under the influence of global warming and intensified human activities, the  
3        meteorological factors across the Loess Plateau have undergone significant  
4        transformations over the past two decades. An analysis of their spatial and temporal  
5        variations reveals complex patterns. Air temperature variations across the region depict  
6        a predominantly increasing trend, with notable exceptions along the northwest-  
7        southeast median and a few isolated areas where decreases are observed (Fig. 8a). The  
8        southern-central part of the plateau experiences the most substantial cooling, exceeding  
9         $-0.06^{\circ}\text{C}/\text{yr}$ , while the western region undergoes the fastest warming, reaching rates of  
10       up to  $0.1^{\circ}\text{C}/\text{yr}$ . Over the past two decades, the mean annual temperature on the Loess  
11       Plateau has stabilized around  $9.32^{\circ}\text{C}$ , albeit with inter-annual fluctuations indicating a  
12       slight increase of  $0.02^{\circ}\text{C}/\text{yr}$  ( $p < 0.1$ ) (Fig. 8b).

13       Specific humidity follows a similar pattern of increase across most of the plateau,  
14       contrasted with a decreasing trend in a small southeastern sector (Fig. 8c). Over the  
15       study period, the annual average specific humidity initially declined slightly during the  
16       first decade, subsequently experiencing a rapid increase, with an average rate of  $1.29$   
17        $\times 10^{-5} \text{ kg/kg/yr}$  ( $p < 0.1$ ) (Fig. 8d). In contrast, surface shortwave radiation exhibits a  
18       marked decreasing trend across the majority of the region, with only a small eastern-  
19       central area showing an upward trajectory (Fig. 8e). The annual average surface  
20       shortwave radiation demonstrates a fluctuating but overall downward trend, decreasing  
21       at a rate of  $-0.18 \text{ W/m}^2/\text{yr}$  (Fig. 8f). Although the number of water grids with increasing  
22       wind speed is comparable to those with decreasing wind speed, the magnitude of the



1 increase is approximately three times larger than the decrease. Hence, the annual  
2 average wind speed displayed a clear upward trend, with a mean increase rate of 0.02  
3 m/s/yr ( $p < 0.05$ ) (Fig. 8h).



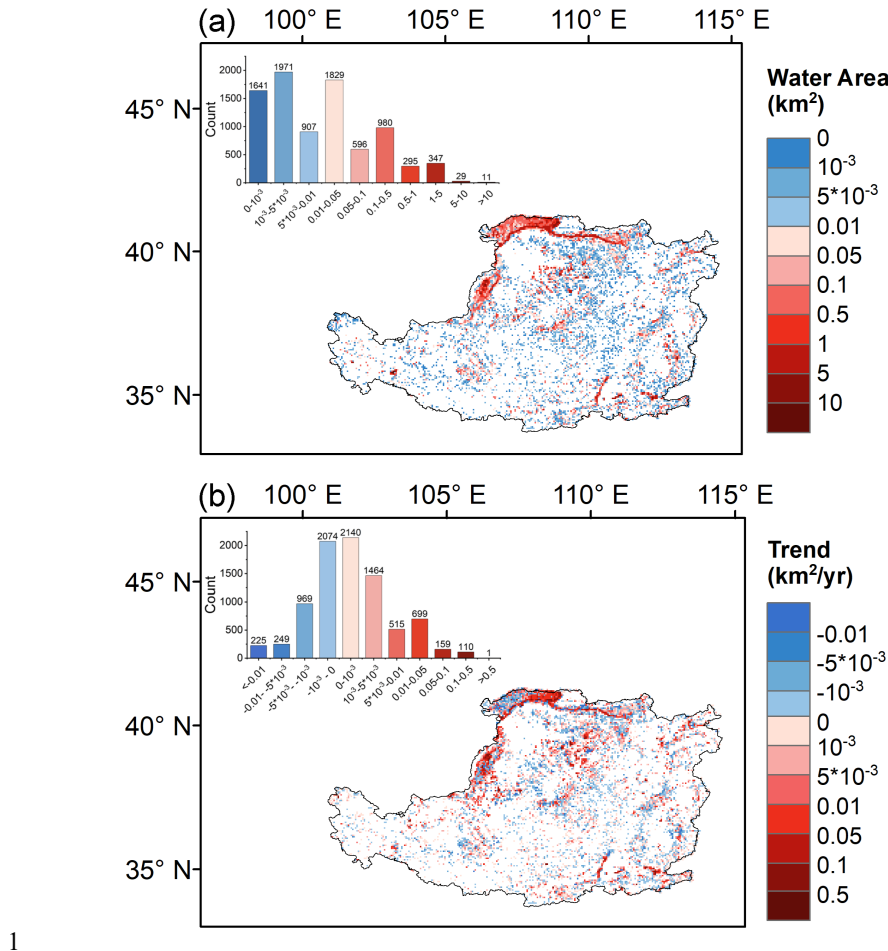
4

5 **Fig. 8.** Average annual trends distribution of (a) temperature, (c) specific humidity, (e)  
6 surface shortwave radiation, and (g) wind speed. Trends in average annual time in (b)



1      temperature, (d) specific humidity, (f) surface shortwave radiation, and (h) wind speed.

2      Compared with meteorological factors, surface water area typically exhibits more  
3      pronounced variations in areas of high human activity. As shown in Figure 9, the surface  
4      water bodies of the Loess Plateau are concentrated in the northwestern region, while  
5      the rest of the region exhibits a more dispersed distribution. Notably, water bodies  
6      smaller than 0.05 km<sup>2</sup> account for 73.8% of all water body grids on the Loess Plateau  
7      (Fig. 9a). Among these, grids showing an increasing trend are nearly 1.5 times those  
8      with a decreasing trend (Fig. 9b). This substantial rate of increase underscores the  
9      dynamic nature of water body expansion in the region. In parallel, there is a more  
10     pronounced trend of growth in the northwestern and central regions, further  
11     emphasizing the significant changes in surface water area over time. This pattern is  
12     consistent with the distribution characteristics of evaporation loss as depicted in Figure  
13     7. Such changes have important implications for the evaporation loss and water  
14     resource allocation, warranting continued evaluation and research.



2 **Fig. 9.** Average distribution and grid count from 2000 to 2018 of (a) water area for 0.05°  
3 grid and (b) the trend of water area.

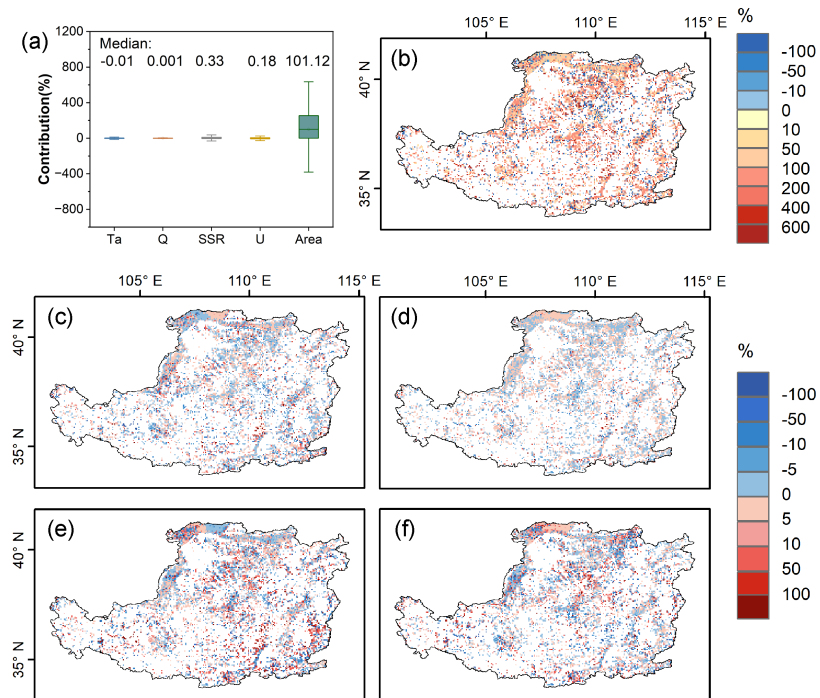
#### 4 3.4.2 Contribution of driving factors

5 To quantify influence of each factor on the evaporation loss, we designed five  
6 detrend experiments that are associated with the water area and the four meteorological  
7 factors as described in subsection 2.4. As shown in Figure 10, the result reveals that  
8 water area variations play a significant role in modulating evaporation processes.



1 Across the study area, changes in water surface area account for a substantial 101.12%  
2 of the variation in evaporation volumes, indicating a strong and positive effect on  
3 evaporation dynamics (Fig. 10a). Spatially, this effect is particularly pronounced on the  
4 Loess Plateau, where water area changes contribute to more than 50% of the  
5 evaporation volume variations in most water bodies (see Fig. 10b). These changes  
6 largely enhance evaporation loss, underscoring the critical role of water body dynamics  
7 in regulating evaporation at both local and regional scales. Notably, the central part of  
8 the Loess Plateau exhibits a noticeable decreasing trend in evaporation volumes, which  
9 can be attributed to the shrinkage of water bodies in this area.

10 In contrast, the influence of meteorological factors on evaporation volumes is  
11 relatively modest. Among these factors, shortwave radiation exhibits the most  
12 significant effect, with a contribution of 0.33%. However, the cumulative effect of all  
13 meteorological factors only accounts for 0.5% of the variation in evaporation volumes,  
14 suggesting potential offsetting trends among these factors. Spatially, the contributions  
15 of meteorological factors to evaporation volumes are either positive or negative but  
16 remain relatively small, with specific humidity contributing below 5% in most regions  
17 and the other three meteorological factors generally contributing less than 10% (Figure  
18 10c-f). The above results emphasize the primary importance of water area dynamics in  
19 regulating evaporation volumes, while meteorological factors play a secondary, albeit  
20 complex role.



1

2 **Fig. 10.** (a) The contributions of factors to the changes in evaporation volume. The  
3 factors considered are air temperature (Ta), specific humidity (Q), surface shortwave  
4 radiation (SSR), wind speed (U), and water area (Area). Changes in evaporation volume  
5 caused by (b) water area, (c) air temperature, (d) specific humidity, (e) surface  
6 shortwave radiation, and (f) wind speed.

7 **4. Discussion**

8 **4.1 Reliability of evaporation estimation**

9 A significant challenge in estimating evaporation rates arises from fluctuations in



1 the heat storage of the water body. The thermal storage of a water body directly  
2 influences its energy contribution and water surface temperature (McMahon et al.,  
3 2013), subsequently impacting evaporation rates (Fairall et al., 1996; Leconte, 2015;  
4 Nehorai et al., 2013). For instance, the incorporation of the thermal storage term in Lake  
5 Mead (Nevada/Arizona) improved the estimated  $R^2$  from 0.29 to 0.84 compared to  
6 models that excluded it (Zhao and Gao, 2019). Furthermore, water depth emerges as a  
7 critical parameter in estimating the heat storage capacity of a water body. In particular,  
8 the median depth in China (31.8 m) is significantly greater than that in the United States  
9 (21.9 m) (Tian et al., 2021). Deeper water bodies, particularly when there is a substantial  
10 temperature difference between air and water, possess a greater heat storage capacity.  
11 This capacity further moderates the disparity between air temperature and water surface  
12 temperature, a factor crucial for accurately estimating the heat storage dynamics related  
13 to water body depth.

14 Incorporating these dynamics is important to provide a more refined estimation of  
15 surface water evaporation (Panin et al., 2006; Wossenu, 2001; Zhang et al., 2024). To  
16 consider the effect of heat storage on evaporation, we developed a modified Penman  
17 model that incorporates the concept of equilibrium temperature, which was successfully  
18 used to estimate the evaporation rate of surface water bodies across Loess Plateau. The  
19 comparison between the simulated evaporation rates and those measured using  
20 evaporation pans reveals a coefficient of determination ( $R^2$ ) of approximately 0.7, with  
21 a relative bias of less than 5 mm/month. This level of agreement underscores the  
22 robustness of our model and its capacity to accurately replicate observed evaporation



1 patterns. Importantly, the averaged evaporation rate estimated for the Loess Plateau in  
2 this study is about 2.98 mm/d, demonstrating excellent consistency with evaporation  
3 rates reported for specific reservoirs or water bodies in the region. For instance,  
4 previous studies focusing on various water bodies within the Loess Plateau have  
5 generally reported evaporation rates falling within the range of 2.73 to 3.72 mm/d  
6 (equivalent to 1000~1358 mm/yr) (Ma Haijiao et al., 2013; Ren and Guo, 2006; Tlan  
7 et al., 2005). This alignment indicates that our methodology, which integrates multiple  
8 physical parameters, is capable of producing evaporation estimates that are in good  
9 agreement with those derived from more localized studies.

10 Particularly noteworthy is the high evaporation rate observed in the northwest  
11 region of the Loess Plateau, reaching 4~5 mm/d. This finding is corroborated by similar  
12 observations from Ding et al. (2012), who reported an evaporation rate of  
13 approximately 4.17 mm/d in the same area. The consistency across these studies,  
14 despite differences in methodologies and study areas, suggests that our approach  
15 captures the spatial variability of evaporation rates within the Loess Plateau, likely  
16 reflecting regional differences in climate and surface water coverage.

17 To further solidify the estimated evaporation loss, we delved into an analysis of  
18 evaporation volume, while few studies have estimated this variable for water bodies in  
19 the Loess Plateau. Among the limited research available, Zhang et al., (2014) estimated  
20 the evaporation loss from the reservoir upstream of Huayuankou at approximately  $4.14 \times 10^6$  m<sup>3</sup>/d (equivalent to  $1.51 \times 10^9$  m<sup>3</sup>/yr). In comparison, our study calculated an  
21 evaporation loss of  $4.16 \times 10^6$  m<sup>3</sup>/d, a value closely aligned with Zhang et al.'s findings.  
22



1 This similarity provides a validation of our estimation methodology, suggesting that  
2 our calculated evaporation loss for the Loess Plateau reservoirs is both reasonable and  
3 reliable. By demonstrating consistency with established results, our findings offer  
4 further confidence in the applicability of our methods to similar hydrological contexts  
5 in the region.

## 6 **4.2 Evaporation variability and its drivers**

7 This study presented the spatiotemporal variations in water body evaporation  
8 across the Loess Plateau. Our findings unveil a distinct spatial pattern, with evaporation  
9 rates consistently higher in the southeastern region compared to the northwestern part.  
10 This spatial distribution aligns closely with the regional climate gradient (Figures 6 and  
11 8), suggesting a strong influence of climatic conditions on evaporation dynamics. The  
12 relatively higher evaporation rates in the northwest can be attributed to stronger surface  
13 shortwave radiation, lower humidity, and potentially higher wind speeds, all of which  
14 favor enhanced evaporation. When examining temporal trends over the past two  
15 decades, our results indicate a subtle yet non-significant decreasing trend in water body  
16 evaporation rates across the Loess Plateau. This trend is primarily driven by changes in  
17 key climatic factors. Specifically, while air temperature and wind speed have shown an  
18 increasing trend (Figure 8), which typically enhances evaporation, these effects have  
19 been counterbalanced by concurrent increases in air humidity and decreases in solar  
20 radiation. The combined impact of these changes has led to a net, albeit modest,  
21 decrease in evaporation rates.



1        As to the evaporation volume, our study unveils a notable increase over the Loess  
2        Plateau during the past two decades, with an ascending rate of  $0.117 \times 10^6 \text{ m}^3/\text{d/yr}$ .  
3        Furthermore, there is a distinct seasonal pattern in the evaporation volume, with peaks  
4        occurring in May and October. The observed upward trend in total water evaporation  
5        can be primarily attributed to the expansion of water bodies within the study area. This  
6        expansion is a direct consequence of the escalating human demand for water across  
7        various sectors, including agriculture, industry, domestic use, and ecological  
8        preservation (Liu et al., 2023). To meet these burgeoning needs, numerous reservoirs  
9        and dams have been constructed, leading to an enlargement of surface water.  
10       Additionally, the proliferation of small check dams, aimed at reducing sediment load in  
11       river channels, has further contributed to the augmentation of water body areas. These  
12       anthropogenic interventions collectively facilitate increased water evaporation losses.

13       Previous studies have explored water evaporation dynamics across various global  
14       regions, revealing significant variations influenced by both natural and anthropogenic  
15       factors. A notable observation is the substantial increase in lake evaporation rates  
16       worldwide, attributed to a 58% rise in evaporation rates coupled with a 23% reduction  
17       in lake ice cover (Zhao et al., 2022). This underscores the profound impact of climate-  
18       related changes, such as rising temperatures and altered precipitation patterns, on lake  
19       evaporation. Furthermore, the proliferation of large reservoirs, particularly in middle-  
20       income countries, has emerged as the primary driver of increased reservoir evaporation  
21       globally (Tian et al., 2022). This highlights the significant role of anthropogenic  
22       interventions, particularly water infrastructure development, in shaping evaporation

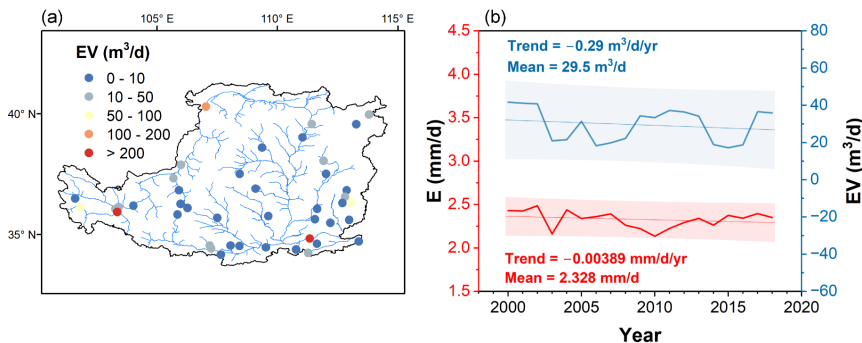


1 trends. Turning to specific regions, studies in the Namoi catchment have shown a  
2 decreasing trend in total evaporation volumes, despite an increasing trend in surface  
3 water evaporation rates. This apparent contradiction has been linked to a reduction in  
4 the frequency of surface water occurrences, indicating that the availability and  
5 persistence of water bodies play a crucial role in modulating evaporation rates (Fuentes  
6 et al., 2020). Similarly, in China, increased evaporation losses from reservoirs have  
7 been attributed to both higher evaporation rates and the expansion of reservoir areas  
8 (Tian et al., 2021).

9 While these studies have contributed to our understanding of water evaporation,  
10 they have primarily focused on large reservoirs or lakes. In contrast, our study  
11 encompasses a comprehensive analysis of all water bodies, including various small-  
12 scale reservoirs and check dams, as well as large reservoirs/lakes in the Loess Plateau  
13 region. To detect the evaporation in large reservoirs in the Loess Plateau, we estimated  
14 48 large reservoirs documented in the GRand database (Lehner et al., 2011,  
15 <http://globaldamwatch.org/>). As shown in Figure 11, the evaporation rate has a slight  
16 decline for the 48 large reservoirs between 2000 and 2018, accompanied by a decrease  
17 in the total evaporation volume ( $-0.29 \text{ m}^3/\text{d}/\text{yr}$ ). This trend of the evaporation rate for the  
18 large reservoirs aligns with the average evaporation rate over the Loess Plateau (Figure  
19 6), but contrasts with the increasing total evaporation volume observed across the entire  
20 region (Figure 7). This discrepancy suggests that small- and medium-sized water bodies  
21 significantly contribute to the overall evaporation on the Loess Plateau. The contrasting  
22 trends between large reservoirs and the broader Loess Plateau highlight the complexity



1 of evaporation dynamics in different water body types and scales.



2

3 **Fig. 11.** (a) The spatial distribution of 48 large reservoirs and their average evaporation  
4 volume. (b) Temporal evaporation rate (E) and evaporation volume (EV) of the 48 large  
5 reservoirs for the period of 2000 to 2018. The shaded area represents 95% prediction  
6 bands.

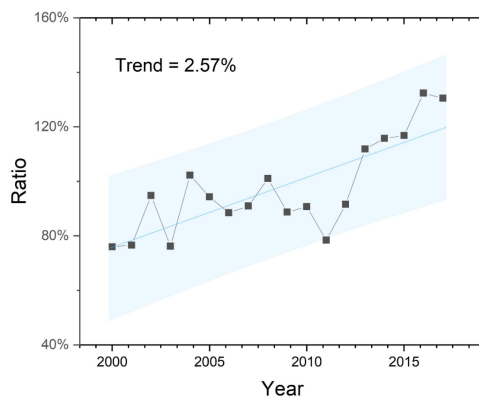
### 7 **4.3 Implications and limitations**

8 Our study, which employs a modified Penman equation that incorporates dynamic  
9 water depth and surface areas, represents a significant advancement in accurately  
10 estimating evaporation rates and volumes for open water bodies. This methodological  
11 refinement underscores the importance of considering both meteorological factors and  
12 the dynamic nature of water bodies, particularly for small- to medium-sized entities.  
13 Ignoring these dynamics, especially for small- and medium-sized water bodies, can lead  
14 to substantial uncertainties in evaporation assessments, with potential ramifications for  
15 regional water balance calculations (Dawidek et al., 2014; Stan et al., 2016).

16 A notable finding from our research is the paradoxical trend of decreasing



1 evaporation rates yet increasing total evaporation volumes on the Loess Plateau. This  
2 finding has profound implications for water resource planning and management in the  
3 region. The extensive construction of various reservoirs globally over the past few  
4 decades aimed at augmenting local water supplies for agricultural irrigation, industrial,  
5 or domestic purposes (Baldassarre et al., 2018; Resources, 2006). However, the  
6 development of the water conservancy projects has potential of exacerbating  
7 evaporation losses—a factor that has largely been overlooked in resource planning. By  
8 comparing water evaporation volumes with surface water withdrawal by residents in  
9 the Loess Plateau (Figure 12), we reveal a striking similarity: the magnitude of total  
10 evaporation loss is comparable with the average annual surface water withdrawal  
11 (approximately  $1.55 \times 10^9$  m<sup>3</sup>/yr). The ratio of evaporation to the withdrawal has  
12 escalated from 80% in 2000 to 130% in 2018, highlighting considerable evaporation  
13 loss and a significant threat to water security in the region. Therefore, future water  
14 project planning needs to incorporate evaporation losses to mitigate potential water  
15 resource risks.





1   **Fig. 12.** The ratio of surface water evaporation volume to annual average water  
2   withdrawal by residents on the Loess Plateau from 2000 to 2017.

3       Previous studies generally focus on large reservoirs or lakes to monitor and  
4   investigate their water budgets (Tian et al., 2021, 2022). This may have inadvertently  
5   underestimated the contribution of smaller water bodies to overall evaporation as  
6   evidenced in this study. These smaller entities are often more sensitive to local climatic  
7   and anthropogenic impacts, necessitating a more granular analysis in future research.  
8       To comprehensively understand and manage water resources, it is imperative to extend  
9   monitoring and modeling efforts to small- and medium-sized water bodies, which our  
10   findings suggest play a pivotal role in the regional evaporation budget.

11       Despite the insights for the methods and findings in our study, several limitations  
12   merit acknowledgment. One notable limitation of our study pertains to the reliance on  
13   the JRC-GSW water body data for calculating water depth and surface area. While this  
14   dataset has been instrumental in our analysis, we did not conduct an independent  
15   assessment of its accuracy and completeness. It is important to highlight that the JRC-  
16   GSW data exhibit seasonal gaps (Liu et al., 2023; Pekel et al., 2016), which could  
17   introduce uncertainties into our calculations of water depth, as well as subsequent  
18   estimations of evaporation rates and volumes. These data absences might reflect  
19   variations in water levels and extents that are not captured by our methodology, thereby  
20   affecting the precision and reliability of our findings. Future research could benefit from  
21   incorporating additional data sources or employing advanced remote sensing  
22   techniques to validate and complement the JRC-GSW dataset, ensuring a more robust



1 representation of water body dynamics across different seasons.

2 Another limitation concerns the evaluation of water body evaporation, which was

3 assessed using evaporation pan data collected near the reservoir. Although this approach

4 provided a practical strategy for validation, it is acknowledged that evaporation rates

5 from pans can significantly diverge from those of various water bodies due to

6 differences in surface characteristics, heat capacity, and exposure to environmental

7 factors. Although adjustments were made to align pan measurements with actual water

8 evaporation conditions, a certain level of uncertainty persists in this extrapolation. To

9 mitigate this limitation and enhance the accuracy of evaporation estimates, future

10 studies should prioritize the deployment of more comprehensive observational

11 networks. This could include installing eddy covariance systems at multiple reservoir

12 levels or employing floating evaporation pans directly on water surfaces to capture

13 more representative evaporation rates. Such methodologies would not only reduce the

14 inherent uncertainties associated with current measurement techniques but also provide

15 a finer spatial and temporal resolution of evaporation processes, ultimately leading to

16 more accurate and reliable model outputs.

## 17 5. Conclusions

18 This study improved the Penman equation to estimate open water evaporation in

19 the Loess Plateau by incorporating an equilibrium temperature approach, with

20 consideration of the variations in surface water area and depth. The improved

21 methodology, validated against adjusted pan evaporation measurements, demonstrated



1 a robust performance with a coefficient of determination exceeding 0.7 and nearly all  
2 biases below 15 mm/month, highlighting its efficacy in simulating evaporation dynamics.

3 Our findings reveal that the average evaporation rate in the Loess Plateau is about  
4 2.98 mm/d over the past two decades, with peak values occurring in May and October,  
5 albeit showing a slight decreasing trend. However, the total evaporation volume or loss  
6 stands at  $4.16 \times 10^6$  m<sup>3</sup>/d, exhibiting a rapid increase at a rate of  $0.117 \times 10^6$  m<sup>3</sup>/d/yr.

7 Attribution analysis further elucidates that the primary driver behind the changes in the  
8 total evaporation volume is the expansion of water surface area, accounting for a  
9 dominant contribution of the variation, while climatic factors play a minor role.  
10 Particularly, the proliferation of small- to medium-sized reservoirs and check dams in  
11 the Loess Plateau has significantly amplified evaporation losses, which are roughly  
12 equivalent to the annual surface water withdrawal in the region.

13 These findings underscore the importance of considering the dynamic aspects of  
14 water surface area and depth in assessing the thermal storage capacity of water bodies  
15 for accurate evaporation estimation. Moreover, they emphasize the necessity of  
16 accounting for evaporation losses in water resource management, particularly in the  
17 context of reservoir construction and operation. Enhanced monitoring and estimation  
18 of evaporation losses from small- to medium-sized reservoirs are crucial to bolster  
19 water security in arid regions like the Loess Plateau. This study thus demonstrates that  
20 the research methods employed are readily extendable to other regions. More  
21 importantly, it contributes novel insights into the intricate relationship between water  
22 body dynamics and evaporation, with implications for sustainable water resources



1 planning and management in the face of climate variability and development of the  
2 hydraulic projects.

### 3 **Data availability**

4 The datasets utilized in this study are publicly available from their respective  
5 official sources: The Joint Research Center (JRC) Global Surface Water dataset (GSW)  
6 can be accessed through Google Earth Engine (GEE) platform  
7 (<https://doi.org/10.1038/nature20584>). The China Meteorological Forcing Dataset  
8 (CMFD) was obtained from the National Tibetan Plateau Data Center  
9 (<https://doi.org/10.11888/AtmosphericPhysics.tpe.249369.file>). ERA5 monthly data  
10 were downloaded from the Copernicus Climate Data Store  
11 (<https://doi.org/10.24381/cds.f17050d7>). The Advanced Spaceborne Thermal Emission  
12 and Reflection Radiometer Global Digital Elevation Model (ASTER GDEM) version  
13 3 data were acquired from NASA's Land Processes Distributed Active Archive Center  
14 (<https://doi.org/10.5067/ASTER/ASTGTM.003>). Meteorological station evaporation  
15 records were provided by the China Meteorological Administration  
16 (<http://data.cma.cn/>). The data generated in this study (evaporation rate and evaporation  
17 volume) can be accessed in a Zenodo repository (<https://zenodo.org/records/14963640>).

### 18 **Author contributions**

19 X.X. and Y.L. designed the study. Y.L. carried out image data processing. Y.L. and  
20 X.X. led interpretation of the results and writing of the manuscript. Y.W., A.T., D.P.,



1 and X.W. contributed to the discussion.

## 2 Competing interests

3 The authors declare that they have no conflict of interest.

## 4 Financial support

5 This study is supported by a grant from the National Natural Science Foundation  
6 of China (No. 42271021).

## 7 Reference

8 Bai, M., Mo, X., Liu, S., and Hu, S.: Contributions of climate change and vegetation  
9 greening to evapotranspiration trend in a typical hilly-gully basin on the Loess Plateau,  
10 China, *Sci. Total Environ.*, 657, 325–339,  
11 <https://doi.org/10.1016/j.scitotenv.2018.11.360>, 2019.

12 Bai, P., Cai, C., Liu, X., Wei, T., and Liu, L.: Estimation of Evaporation Losses from  
13 Reservoirs in the Upper Yellow River, *J. China Hydrol.*, 43, 86-90+110,  
14 <https://doi.org/10.19797/j.cnki.1000-0852.20220332>, 2023.

15 Baldassarre, G. Di, Wanders, N., Aghakouchak, A., Kuil, L., Rangecroft, S., Veldkamp,  
16 T. I. E., Garcia, M., Oel, P. R. Van, Breinl, K., and Loon, A. F. Van: Water shortages  
17 worsened by reservoir effects, *Nat. Sustain.*, 1, 617–622,  
18 <https://doi.org/10.1038/s41893-018-0159-0>, 2018.

19 De Bruin, H. A. R.: Temperature and energy balance of a water reservoir determined  
20 from standard weather data of a land station, *J. Hydrol.*, 59, 261–274,  
21 [https://doi.org/https://doi.org/10.1016/0022-1694\(82\)90091-9](https://doi.org/https://doi.org/10.1016/0022-1694(82)90091-9), 1982.

22 Dawidek, J., Ferencz, B., and Conservation, N.: Water balance of selected floodplain  
23 lake basins in the Middle Bug River valley, 1457–1465, <https://doi.org/10.5194/hess-18-1457-2014>, 2014.

25 Deng, H., Tang, Q., Yun, X., Tang, Y., Liu, X., Xu, X., Sun, S., Zhao, G., Zhang, Y.,  
26 and Zhang, Y.: Wetting trend in Northwest China reversed by warmer temperature and  
27 drier air, *J. Hydrol.*, 613, 128435, <https://doi.org/10.1016/j.jhydrol.2022.128435>, 2022.

28 Ding, L., Liu, T., Zhang, H., Li, C., and Tong, X.: Analysis of Water Evaporation of  
29 Inner Mongolia Section of the Yellow River (in Chinese) , *YELLOW RIVER*, 34, 38–  
30 40, 2012.



1 Edinger, J. E., Duttweiler, D. W., and Geyer, J. C.: The Response of Water  
2 Temperatures to Meteorological Conditions, *Water Resour. Res.*, 4, 1137–1143,  
3 https://doi.org/10.1029/WR004i005p01137, 1968.

4 Fairall, C. W., Bradley, E. F., Rogers, D. P., Edson, J. B., and Young, G. S.: Bulk  
5 parameterization of air-sea fluxes for tropical ocean-atmosphere coupled-ocean  
6 atmosphere response experiment, *J. Geophys. Res. Ocean.*, 101, 3747–3764,  
7 https://doi.org/10.1029/95JC03205, 1996.

8 Friedrich, K., Grossman, R. L., Huntington, J., Blanken, P. D., Lenters, J., Holman, K.  
9 L. D., Gochis, D., Livneh, B., Prairie, J., Skeie, E., Healey, N. C., Dahm, K., Pearson,  
10 C., Finnessey, T., Hook, S. J., and KowaLsKi, T.: Reservoir evaporation in the Western  
11 United States, *Bull. Am. Meteorol. Soc.*, 99, 167–187, https://doi.org/10.1175/BAMS-  
12 D-15-00224.1, 2018.

13 Fu, B., Wang, S., Liu, Y., Liu, J., Liang, W., and Miao, C.: Hydrogeomorphic  
14 Ecosystem Responses to Natural and Anthropogenic Changes in the Loess Plateau of  
15 China, *Annu. Rev. Earth Planet. Sci.*, 45, 223–243, https://doi.org/10.1146/annurev-  
16 earth-063016-020552, 2017.

17 Fuentes, I., van Ogtrop, F., and Vervoort, R. W.: Long-term surface water trends and  
18 relationship with open water evaporation losses in the Namoi catchment, Australia, *J. Hydrol.*, 584, 124714, https://doi.org/10.1016/j.jhydrol.2020.124714, 2020.

20 Guan, X. and Mascaro, G.: Impacts of climate change on the food-water nexus in  
21 central Arizona, *Agric. For. Meteorol.*, 333, 109413,  
22 https://doi.org/10.1016/j.agrformet.2023.109413, 2023.

23 Guo, Y., Zhang, Y., Ma, N., Xu, J., and Zhang, T.: Long-term changes in evaporation  
24 over Siling Co Lake on the Tibetan Plateau and its impact on recent rapid lake  
25 expansion, *Atmos. Res.*, 216, 141–150, https://doi.org/10.1016/j.atmosres.2018.10.006,  
26 2019.

27 He, J., Yang, K., Tang, W., Lu, H., Qin, J., Chen, Y., and Li, X.: The first high-  
28 resolution meteorological forcing dataset for land process studies over China, *Sci. Data*,  
29 7, 1–11, https://doi.org/10.1038/s41597-020-0369-y, 2020.

30 Hersbach, H., Bell, B., Berrisford, P., Hirahara, S., Horányi, A., Muñoz-Sabater, J.,  
31 Nicolas, J., Peubey, C., Radu, R., Schepers, D., Simmons, A., Soci, C., Abdalla, S.,  
32 Abellan, X., Balsamo, G., Bechtold, P., Biavati, G., Bidlot, J., Bonavita, M., De Chiara,  
33 G., Dahlgren, P., Dee, D., Diamantakis, M., Dragani, R., Flemming, J., Forbes, R.,  
34 Fuentes, M., Geer, A., Haimberger, L., Healy, S., Hogan, R. J., Hólm, E., Janisková,  
35 M., Keeley, S., Laloyaux, P., Lopez, P., Lupu, C., Radnoti, G., de Rosnay, P., Rozum,  
36 I., Vamborg, F., Villaume, S., and Thépaut, J. N.: The ERA5 global reanalysis, *Q. J. R. Meteorol. Soc.*, 146, 1999–2049, https://doi.org/10.1002/qj.3803, 2020.

38 Hollinger, D. Y. and Richardson, A. D.: Uncertainty in eddy covariance measurements  
39 and its application to physiological models, *Tree Physiol.*, 25, 873–885,  
40 https://doi.org/10.1093/treephys/25.7.873, 2005.

41 Jensen, M. E.: Estimating evaporation from water surfaces, in: CSU/ARS  
42 Evapotranspiration Workshop, Fort Collins, CO, 1–27, 2010.

43 Jian, S., Zhao, C., Fang, S., and Yu, K.: Effects of different vegetation restoration on  
44 soil water storage and water balance in the Chinese Loess Plateau, *Agric. For. Meteorol.*,



1 206, 85–96, <https://doi.org/10.1016/j.agrformet.2015.03.009>, 2015.

2 Jiang, C., Zhang, H., Wang, X., Feng, Y., and Labzovskii, L.: Challenging the land  
3 degradation in China's Loess Plateau: Benefits, limitations, sustainability, and adaptive  
4 strategies of soil and water conservation, *Ecol. Eng.*, 127, 135–150,  
5 <https://doi.org/10.1016/j.ecoleng.2018.11.018>, 2019.

6 Jiang, F., Xie, X., Liang, S., Wang, Y., Zhu, B., Zhang, X., and Chen, Y.: Loess Plateau  
7 evapotranspiration intensified by land surface radiative forcing associated with  
8 ecological restoration, *Agric. For. Meteorol.*, 311, 108669,  
9 <https://doi.org/10.1016/j.agrformet.2021.108669>, 2021.

10 Jiang, F., Xie, X., Wang, Y., Liang, S., Zhu, B., Meng, S., Zhang, X., Chen, Y., and  
11 Liu, Y.: Vegetation greening intensified transpiration but constrained soil evaporation  
12 on the Loess Plateau, *J. Hydrol.*, 614, 128514,  
13 <https://doi.org/10.1016/j.jhydrol.2022.128514>, 2022.

14 Jin, Z., Liang, W., Yang, Y., Zhang, W., Yan, J., Chen, X., Li, S., and Mo, X.:  
15 Separating Vegetation Greening and Climate Change Controls on Evapotranspiration  
16 trend over the Loess Plateau, *Sci. Rep.*, 7, 1–15, <https://doi.org/10.1038/s41598-017-08477-x>, 2017.

18 Jinhui, W. U. and Zhanbin, L. I.: Advances and prospect of research on water surface  
19 evaporation, *J. Water Resour. Archit. Eng.*, 5, 46–50, 2007.

20 Leconte, J.: TAHOE : STATE OF THE L AKE REPORT 2013 John LeConte, 2015,  
21 2015.

22 Lehner, B., Liermann, C. R., Revenga, C., Vörösmarty, C., Fekete, B., Crouzet, P.,  
23 Döll, P., Endejan, M., Frenken, K., Magome, J., Nilsson, C., Robertson, J. C., Rödel,  
24 R., Sindorf, N., and Wisser, D.: High-resolution mapping of the world's reservoirs and  
25 dams for sustainable river-flow management, *Front. Ecol. Environ.*, 9, 494–502,  
26 <https://doi.org/10.1890/100125>, 2011.

27 Lei, N., Zhou, Z., Zhuang, Q., Chen, W., Chalov, S., Liu, S., Gao, L., and Dong, G.:  
28 Performance Evaluation and Improvement of CMFD's Precipitation Products Over  
29 Shanghai City, China, *Earth Sp. Sci.*, 10, <https://doi.org/10.1029/2022EA002690>, 2023.

30 Li, Q., Luo, Z., Zhong, B., and Zhou, H.: An improved approach for evapotranspiration  
31 estimation usingwater balance equation: Case study of Yangtze River Basin, *Water*  
32 (Switzerland), 10, 1–21, <https://doi.org/10.3390/w10060812>, 2018.

33 Li, Y., Gao, H., Zhao, G., and Tseng, K. H.: A high-resolution bathymetry dataset for  
34 global reservoirs using multi-source satellite imagery and altimetry, *Remote Sens.*  
35 *Environ.*, 244, 111831, <https://doi.org/10.1016/j.rse.2020.111831>, 2020.

36 Li, Y., Zhao, G., Allen, G. H., and Gao, H.: Diminishing storage returns of reservoir  
37 construction, *Nat. Commun.*, 14, <https://doi.org/10.1038/s41467-023-38843-5>, 2023.

38 Li, Z., Liu, W. zhao, Zhang, X. chang, and Zheng, F. li: Impacts of land use change and  
39 climate variability on hydrology in an agricultural catchment on the Loess Plateau of  
40 China, *J. Hydrol.*, 377, 35–42, <https://doi.org/10.1016/j.jhydrol.2009.08.007>, 2009.

41 Liu, F., Li, X., Shi, F., Yang, Y., Liu, M., and Cao, G.: Stable isotopes reveal soil  
42 evaporation and its controlling factors in the Heihe River source area on the  
43 northeastern Qinghai-Tibetan Plateau, *J. Hydrol. Reg. Stud.*, 54, 101901,  
44 <https://doi.org/10.1016/j.ejrh.2024.101901>, 2024.



1 Liu, H., Zhang, Q., and Dowler, G.: Environmental controls on the surface energy  
2 budget over a large Southern Inland water in the united states: An analysis of one-year  
3 eddy covariance flux data, *J. Hydrometeorol.*, 13, 1893–1910,  
4 https://doi.org/10.1175/JHM-D-12-020.1, 2012.

5 Liu, Y., Xie, X., Tursun, A., Wang, Y., Jiang, F., and Zheng, B.: Surface water  
6 expansion due to increasing water demand on the Loess Plateau, *J. Hydrol. Reg. Stud.*,  
7 49, 101485, https://doi.org/10.1016/j.ejrh.2023.101485, 2023.

8 Ma Haijiao et al.: Analysis on Variation Characteristics of Pan Evaporation in Recent  
9 34 Years in the Loess Plateau (in Chinese) , *J. Anhui Agric. Sci.*, 41, 4506–4509, 2013.

10 McJannet, D. L., Webster, I. T., and Cook, F. J.: Environmental Modelling & Software  
11 An area-dependent wind function for estimating open water evaporation using land-  
12 based meteorological data, *Environ. Model. Softw.*, 31, 76–83,  
13 https://doi.org/10.1016/j.envsoft.2011.11.017, 2012.

14 McJannet, D. L., Webster, I. T., Stenson, M. P., and Sherman, B. S.: Estimating open  
15 water evaporation for the Murray-Darling Basin: A report to the Australian Government  
16 from the CSIRO Murray-Darling Basin Sustainable Yields Project, A Rep. to Aust.  
17 Gov. from CSIRO Murray-Darling Basin Sustain. Yields Proj., 50, 2008.

18 McMahon, T. A., Peel, M. C., Lowe, L., Srikanthan, R., and McVicar, T. R.: Estimating  
19 actual, potential, reference crop and pan evaporation using standard meteorological data:  
20 A pragmatic synthesis, *Hydrol. Earth Syst. Sci.*, 17, 1331–1363,  
21 https://doi.org/10.5194/hess-17-1331-2013, 2013.

22 Milly, P. C. D. and Dunne, K. A.: Colorado River flow dwindle as warming-driven  
23 loss of reflective snow energizes evaporation, *Science* (80- .), 367, 1252–1255,  
24 https://doi.org/10.1126/science.aax0194, 2020.

25 Nehorai, R., Lensky, N., Brenner, S., and Lensky, I.: The dynamics of the skin  
26 temperature of the dead sea, *Adv. Meteorol.*, 2013,  
27 https://doi.org/10.1155/2013/296714, 2013.

28 Panin, G. N., Nasonov, A. E., Foken, T., and Lohse, H.: On the parameterisation of  
29 evaporation and sensible heat exchange for shallow lakes, *Theor. Appl. Climatol.*, 85,  
30 123–129, https://doi.org/10.1007/s00704-005-0185-5, 2006.

31 Pekel, J. F., Cottam, A., Gorelick, N., and Belward, A. S.: High-resolution mapping of  
32 global surface water and its long-term changes, *Nature*, 540, 418–422,  
33 https://doi.org/10.1038/nature20584, 2016.

34 Peng, D., Xie, X., Liang, S., Wang, Y., Tursun, A., Liu, Y., Jia, K., Ma, H., and Chen,  
35 Y.: Improving evapotranspiration partitioning by integrating satellite vegetation  
36 parameters into a land surface model, *J. Hydrol.*, 643, 131928,  
37 https://doi.org/10.1016/j.jhydrol.2024.131928, 2024.

38 Ren, G. Y. and Guo, J.: Change in pan evaporation and the influential factors over  
39 China: 1956–2000, *J. Nat. Resour.*, 21, 31–44, 2006.

40 Resources, F.: Global Hydrological Cycles and, 1068–1073, 2006.

41 Rotstayn, L. D., Roderick, M. L., and Farquhar, G. D.: A simple pan-evaporation model  
42 for analysis of climate simulations: Evaluation over Australia, *Geophys. Res. Lett.*, 33,  
43 1–5, https://doi.org/10.1029/2006GL027114, 2006.

44 Sheng, Q., Shen, S. H., and Gu, Z.: Conversion coefficient between small evaporation



1 pan and theoretically calculated water surface evaporation in China, *J. Nanjing Inst.*  
2 *Meteorol.*, 30, 561–565, 2007.

3 Shi, C., Niu, K., Chen, T., and Zhu, X.: THE STUDY OF PAN COEFFICIENTS OF  
4 EVAPORATION PANS OF WATER, *Sci. Geogr. Sin.*, 6, 305–313,  
5 https://doi.org/10.13249/j.cnki.sgs.1986.04.305, 1986.

6 Stan, F., Neculau, G., Zaharia, L., and Ioana-, G.: Study on the evaporation and  
7 evapotranspiration measured on the Căldărușani Lake (Romania), *Procedia Environ.*  
8 *Sci.*, 32, 281–289, https://doi.org/10.1016/j.proenv.2016.03.033, 2016.

9 Sun, Q., Miao, C., Duan, Q., and Wang, Y.: Temperature and precipitation changes  
10 over the Loess Plateau between 1961 and 2011, based on high-density gauge  
11 observations, *Glob. Planet. Change*, 132, 1–10,  
12 https://doi.org/10.1016/j.gloplacha.2015.05.011, 2015.

13 Tan, Q., Xu, Z., Zoha, Y., Liu, J., Ban, C., Liu, X., and Wang, J.: Applicability of China  
14 meteorological forcing dataset to the Nianchu River basin, *J. Beijing Norm. Univ. Sci.*,  
15 57, 372–379, https://doi.org/10.12202/j.0476-0301.2020261, 2021.

16 Tanny, J., Cohen, S., Assouline, S., Lange, F., Grava, A., Berger, D., Teltch, B., and  
17 Parlange, M. B.: Evaporation from a small water reservoir: Direct measurements and  
18 estimates, *J. Hydrol.*, 351, 218–229, https://doi.org/10.1016/j.jhydrol.2007.12.012,  
19 2008.

20 Tian, W., Liu, X., Wang, K., Bai, P., Liu, C., and Liang, X.: Estimation of reservoir  
21 evaporation losses for China, *J. Hydrol.*, 607,  
22 https://doi.org/10.1016/j.jhydrol.2021.126142, 2021.

23 Tian, W., Liu, X., Wang, K., Bai, P., Liu, C., and Liang, X.: Estimation of global  
24 reservoir evaporation losses, *J. Hydrol.*, 607, 127524,  
25 https://doi.org/10.1016/j.jhydrol.2022.127524, 2022.

26 Tlan, J., Cui, Q., and Xu, J.: Surface-evaporation of large and middle reservoirs affects  
27 the cunount of water resource in the Yellow River valley, *JOURNAL-SHANDONG*  
28 *Agric. Univ.*, 36, 391, 2005.

29 Vishwakarma, D. K., Pandey, K., Kaur, A., Kushwaha, N. L., Kumar, R., Ali, R.,  
30 Elbeltagi, A., and Kuriqi, A.: Methods to estimate evapotranspiration in humid and  
31 subtropical climate conditions, *Agric. Water Manag.*, 261, 107378,  
32 https://doi.org/10.1016/j.agwat.2021.107378, 2022.

33 Vystavna, Y., Harjung, A., Monteiro, L. R., Matiatos, I., and Wassenaar, L. I.: Stable  
34 isotopes in global lakes integrate catchment and climatic controls on evaporation, *Nat.*  
35 *Commun.*, 12, 1–7, https://doi.org/10.1038/s41467-021-27569-x, 2021.

36 Wang, D., Wang, D., Mei, Y., Yang, Q., Ji, M., Li, Y., Liu, S., Li, B., Huang, Y., and  
37 Mo, C.: Estimates of the Land Surface Hydrology from the Community Land Model  
38 Version 5 (CLM5) with Three Meteorological Forcing Datasets over China, *Remote*  
39 *Sens.*, 16, 1–30, https://doi.org/10.3390/rs16030550, 2024.

40 Wang, J., Liu, H., and Shen, L.: An Observational and Modeling Study of Inverse-  
41 Temperature Layer and Water Surface Heat Flux, *Geophys. Res. Lett.*, 50, 1–10,  
42 https://doi.org/10.1029/2023GL104358, 2023.

43 Wang, Z., Chen, Z., Yu, S., Zhang, Q., Wang, Y., and Hao, J.: Erosion-control  
44 mechanism of sediment check dams on the Loess Plateau, *Int. J. Sediment Res.*, 36,



1 668–677, <https://doi.org/10.1016/j.ijsrc.2021.02.002>, 2021.

2 Woolway, R. I., Kraemer, B. M., Lenters, J. D., Merchant, C. J., O'Reilly, C. M., and  
3 Sharma, S.: Global lake responses to climate change, *Nat. Rev. Earth Environ.*, 1, 388–  
4 403, <https://doi.org/10.1038/s43017-020-0067-5>, 2020.

5 Wossennu, A.: Evaporation Estimation for Lake Okeechobee in South Florida, *J. Irrig.  
6 Drain. Eng.*, 127, 140–147, [https://doi.org/10.1061/\(ASCE\)0733-  
9437\(2001\)127:3\(140\)](https://doi.org/10.1061/(ASCE)0733-<br/>7 9437(2001)127:3(140)), 2001.

8 Wu, D., Xie, X., Tong, J., Meng, S., and Wang, Y.: Sensitivity of Vegetation Growth  
9 to Precipitation in a Typical Afforestation Area in the Loess Plateau: Plant-Water  
10 Coupled Modelling, *Ecol. Modell.*, 430, 109128,  
11 <https://doi.org/10.1016/j.ecolmodel.2020.109128>, 2020.

12 Xiao, J., Wang, L., Deng, L., and Jin, Z.: Characteristics, sources, water quality and  
13 health risk assessment of trace elements in river water and well water in the Chinese  
14 Loess Plateau, *Sci. Total Environ.*, 650, 2004–2012,  
15 <https://doi.org/10.1016/j.scitotenv.2018.09.322>, 2019.

16 Xie, X., Liang, S., Yao, Y., Jia, K., Meng, S., and Li, J.: Detection and attribution of  
17 changes in hydrological cycle over the Three-North region of China: Climate change  
18 versus afforestation effect, *Agric. For. Meteorol.*, 203, 74–87,  
19 <https://doi.org/10.1016/j.agrformet.2015.01.003>, 2015.

20 Yang, K., Yu, Z., Luo, Y., Zhou, X., and Shang, C.: Spatial-Temporal Variation of Lake  
21 Surface Water Temperature and Its Driving Factors in Yunnan-Guizhou Plateau, *Water  
22 Resour. Res.*, 55, 4688–4703, <https://doi.org/10.1029/2019WR025316>, 2019.

23 Zhang, G., Yao, T., Chen, W., Zheng, G., Shum, C. K., Yang, K., Piao, S., Sheng, Y.,  
24 Yi, S., Li, J., O'Reilly, C. M., Qi, S., Shen, S. S. P., Zhang, H., and Jia, Y.: Regional  
25 differences of lake evolution across China during 1960s–2015 and its natural and  
26 anthropogenic causes, *Remote Sens. Environ.*, 221, 386–404,  
27 <https://doi.org/10.1016/j.rse.2018.11.038>, 2019a.

28 Zhang, J., Ge, Y., Yuan, G., and Song, Z.: Consideration of high-quality development  
29 strategies for soil and water conservation on the loess plateau, *Sci. Rep.*, 12, 1–13,  
30 <https://doi.org/10.1038/s41598-022-12006-w>, 2022.

31 Zhang, K., Xie, X., Zhu, B., Meng, S., and Yao, Y.: Unexpected groundwater recovery  
32 with decreasing agricultural irrigation in the Yellow River Basin, *Agric. Water Manag.*,  
33 213, 858–867, <https://doi.org/10.1016/j.agwat.2018.12.009>, 2019b.

34 Zhang, L., Sun, J., Tian, Y., Zhao, ru, Wang, C., and Guo, fei: Evaporation Loss of  
35 the Water Storage Projects in the Region Above Huayuankou of the Yellow River (in  
36 Chinese) , *YELLOW RIVER*, 36, 95–96, 2014.

37 Zhang, Y., Li, X., Chang, X., Jin, H., Huang, A., Liang, J., Cheng, G., and Wang, X.:  
38 Sensitivity of simulated frozen ground temperatures to different solar radiation and air  
39 temperature products—a case study in the Qilian Mountains in West China, *Permafro.  
40 Periglac. Process.*, 34, 513–529, <https://doi.org/10.1002/ppp.2187>, 2023.

41 Zhang, Z., Tang, Q., Zhao, G., Gaffney, P. P. J., and Dubois, N.: Lake depth, a key  
42 parameter regulating evaporation in semi-arid regions: A case study from Dali Lake,  
43 China, *Hydrol. Process.*, 38, <https://doi.org/10.1002/hyp.15196>, 2024.

44 Zhao, G. and Gao, H.: Estimating reservoir evaporation losses for the United States:



- 1 Fusing remote sensing and modeling approaches, *Remote Sens. Environ.*, 226, 109–
- 2 124, <https://doi.org/10.1016/j.rse.2019.03.015>, 2019.
- 3 Zhao, G., Mu, X., Wen, Z., Wang, F., and Gao, P.: Soil erosion, conservation, and eco-  
4 environment changes in the loess plateau of china, *L. Degrad. Dev.*, 24, 499–510,  
5 <https://doi.org/10.1002/ldr.2246>, 2013.
- 6 Zhao, G., Li, Y., Zhou, L., and Gao, H.: Evaporative water loss of 1.42 million global  
7 lakes, *Nat. Commun.*, 13, 1–10, <https://doi.org/10.1038/s41467-022-31125-6>, 2022.
- 8 Zhou, F., Bo, Y., Ciais, P., Dumas, P., Tang, Q., Wang, X., Liu, J., Zheng, C., Polcher,  
9 J., Yin, Z., Guimbertea, M., Peng, S., Ottle, C., Zhao, X., Zhao, J., Tan, Q., Chen, L.,  
10 Shen, H., Yang, H., Piao, S., Wang, H., and Wada, Y.: Deceleration of China's human  
11 water use and its key drivers, *Proc. Natl. Acad. Sci. U. S. A.*, 117, 7702–7711,  
12 <https://doi.org/10.1073/pnas.1909902117>, 2020.